Cell PRESS

Developmental Cell
Short Article

The Plasma Membrane Flattens Out to Fuel Cell-Surface Growth during *Drosophila* Cellularization

Lauren Figard,[1,2] Heng Xu,[1,3] Hernan G. Garcia,[4] Ido Golding,[1,3,5] and Anna Marie Sokac[1,2,*]
[1]Verna and Marrs McLean Department of Biochemistry and Molecular Biology, Baylor College of Medicine, Houston, TX 77030, USA
[2]Integrative Molecular and Biomedical Sciences Graduate Program, Baylor College of Medicine, Houston, TX 77030, USA
[3]Center for the Physics of Living Cells, University of Illinois at Urbana-Champaign, Urbana, IL 61801, USA
[4]Department of Physics, Princeton University, Princeton, NJ 08544, USA
[5]Center for Theoretical Biological Physics, Rice University, Houston, TX 77005, USA
*Correspondence: sokac@bcm.edu
http://dx.doi.org/10.1016/j.devcel.2013.11.006

SUMMARY

Cell-shape change demands cell-surface growth, but how growth is fueled and choreographed is still debated. Here we use cellularization, the first complete cytokinetic event in *Drosophila* embryos, to show that cleavage furrow ingression is kinetically coupled to the loss of surface microvilli. We modulate furrow kinetics with RNAi against the Rho1-GTPase regulator *slam* and show that furrow ingression controls the rate of microvillar depletion. Finally, we directly track the microvillar membrane and see it move along the cell surface and into ingressing furrows, independent of endocytosis. Together, our results demonstrate that the kinetics of the ingressing furrow regulate the utilization of a microvillar membrane reservoir. Because membranes of the furrow and microvilli are contiguous, we suggest that ingression drives unfolding of the microvilli and incorporation of microvillar membrane into the furrow. We conclude that plasma membrane folding/unfolding can contribute to the cell-shape changes that promote embryonic morphogenesis.

INTRODUCTION

Microvilli are finger-like membrane protrusions that coat the surface of cells. Each finger has a core of bundled actin filaments (F-actin) supporting its shape (DeRosier and Tilney, 2000). Microvilli are found on most cell types, from polarized epithelia of kidney, liver, and lung to neurosensory cells, Schwann cells, immune cells, and embryos (Revenu et al., 2004). Accordingly, the functions attributed to microvilli are wide ranging: microvilli increase surface area to promote absorption of water in the kidney, exposure of digestive enzymes in the gut, and adhesion of lymphocytes to vessel walls (Ashworth and Molitoris, 1999; Louvard et al., 1992; Sundd et al., 2011). In highly specialized forms, microvillar protrusions, like stereocilia in the inner ear, mediate mechanotransduction (Hudspeth and Corey, 1977). In addition, there is a long-standing idea that microvilli serve as a reservoir of excess membrane that can be used for cell-surface growth in events such as cytokinesis, wound healing, morphogenesis, osmotic regulation, cell spreading, and phagocytosis (Arnold, 1969; Bement et al., 1993; Betchaku and Trinkaus, 1978; Ducibella et al., 1977; Fullilove and Jacobson, 1971; Herant et al., 2005; Porter et al., 1973). However, this idea is controversial (Schroeder, 1978; Shuster and Burgess, 2002; Turner and Mahowald, 1976), largely because the data supporting it only demonstrate the presence and absence of microvilli before and after cell-surface growth. What is more, no mechanisms have been revealed to show how membrane shuttles from microvilli to other cell-surface features.

Drosophila cellularization offers perhaps the most dramatic example of cell-surface growth for which the model of microvilli as membrane reservoir has been invoked (Fullilove and Jacobson, 1971; Sommi et al., 2010). In these embryos, the first 13 mitoses proceed with no intervening cytokinesis, generating a syncytium containing ~6,000 cortically anchored nuclei. Then, at interphase of cell cycle 14, plasma membrane furrows simultaneously ingress around every nucleus to build a sheet of epithelial cells (Foe et al., 1993). Cellularization takes ~60 min and cleavage furrows ingress 35 μm, cutting straight into the cytoplasm. Consequently, the surface area of the embryo expands ~25-fold (Lecuit and Wieschaus, 2000). Thus, there is an immediate demand for a huge amount of new membrane. Microvilli decorate the surface of the embryo before cellularization, but are gone by the end of the process (Fabrowski et al., 2013; Fullilove and Jacobson, 1971). So, whereas some have advocated that the new membrane comes from exocytosis of vesicles from internal sources (Lecuit and Wieschaus, 2000), others have proposed that furrow ingression is fueled by the depletion of microvilli (Fullilove and Jacobson, 1971; Sommi et al., 2010).

In this work, we show that the kinetics of microvillar depletion are regulated by furrow ingression throughout cellularization, and we provide evidence for a mechanism where membrane from microvilli moves along the plane of the plasma membrane and into growing cleavage furrows. Because the membrane of the furrow and microvilli are contiguous, we suggest that furrow ingression unfolds and pulls the microvillar membrane into the furrow.

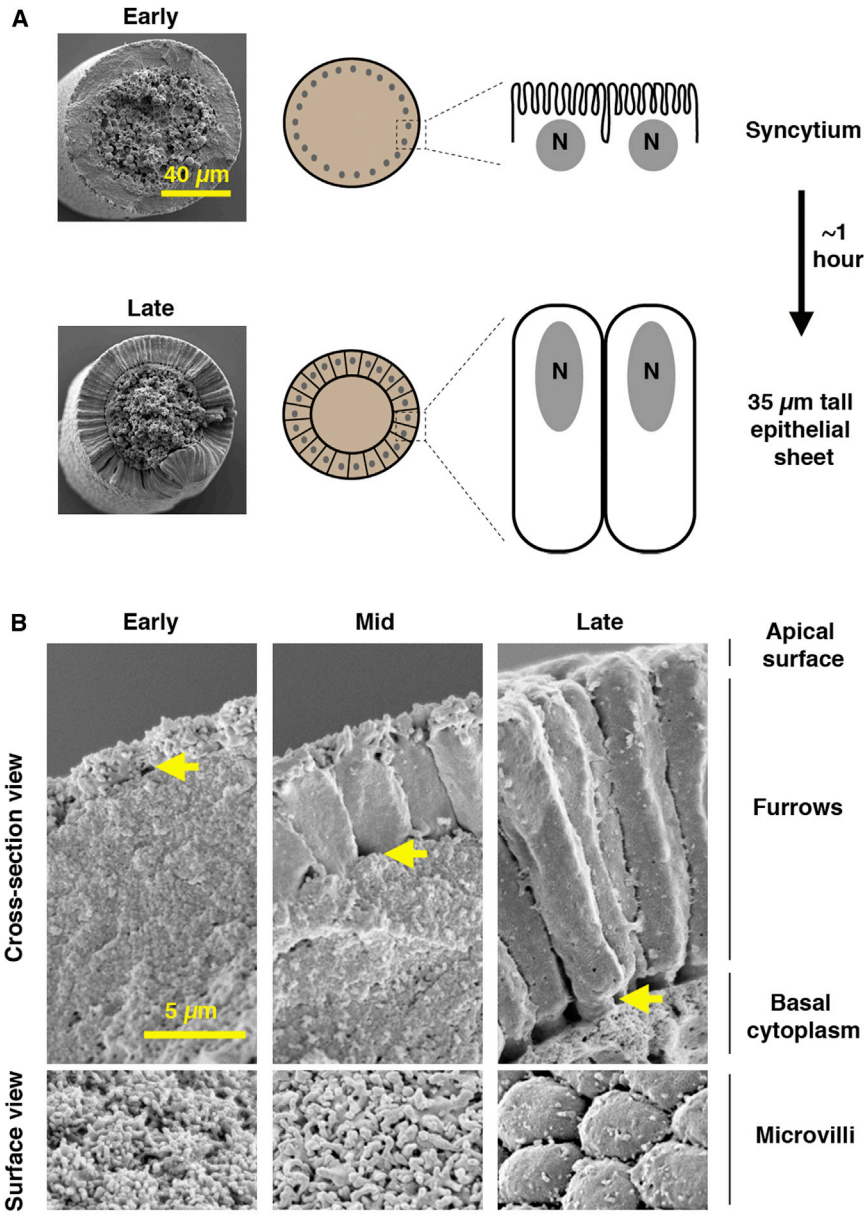

C

Membrane area required for furrow ingression	Area supplied by MV: minimum	Area supplied by MV: maximum
~580 μm^2	243 ± 94 μm^2 (42 ± 16%)	377 ± 50 μm^2 (65 ± 9%)

Figure 1. Microvilli Contain a Large Fraction of Membrane Required for Furrow Ingression

(A) SEM images showing cross-sections of fractured embryos at early/late cellularization, with schematics depicting the same stages. Apical microvilli are depleted as membrane furrows ingress to package nuclei (N) into cells.

(B) SEM images showing microvilli from embryos throughout cellularization. Furrow tips are indicated (arrows).

(C) Estimates for how much furrow membrane the microvilli (MV) could provide (mean ± SD).

See also Figure S1 and Table S1.

RESULTS

Microvilli Can Provide a Significant Fraction of Membrane for Furrow Ingression

Microvilli decorate the surface of embryos before cellularization, but are gone by the end of the process (Figures 1A and 1B; Fabrowski et al., 2013; Fullilove and Jacobson, 1971). So how much furrow membrane can microvilli actually store? We used scanning electron microscopy (SEM) to quantify the density and morphology of microvilli in embryos at early cellularization. For staging, embryos were fractured so that the length of cellularization furrows could be measured (Figure 1B). At short furrow lengths (i.e., early cellularization), SEM images show the apical surface densely packed with microvilli (Figure 1B). Microvillar morphology is heterogeneous, with finger-like projections often emerging from a wider base of membrane, consistent with the dimensions and morphology described for microvilli in a variety of embryos and mammalian cells (Figure S1 available online; Table S1; Ducibella et al., 1977; Revenu et al., 2004).

To estimate the upper and lower limits of membrane area stored in microvilli, we did minimum and maximum calculations based on the observed morphologies (Figure S1). For a minimum, we used the simplest morphology that we saw: a finger-like projection with constant diameter from tip to base (Figure S1A). For a maximum, we used the most elaborate morphology: a hand-like projection with five fingers atop a wide ruffle-like base (Figure S1B). Assuming that every microvillus has either the finger or hand morphology, then ~42% or ~65% of furrow membrane, respectively, could be liberated from microvilli (Figure 1C). Because cells are decorated by a mix of finger and hand morphologies, we suggest that the actual value is somewhere in between. Thus, a snapshot view from early cellularization shows that microvilli contain much of the membrane required for furrow ingression.

The Kinetics of Microvillar Depletion and Furrow Ingression Are the Same

We next examined the timing of microvillar membrane depletion in live cellularizing embryos. We used three-dimensional

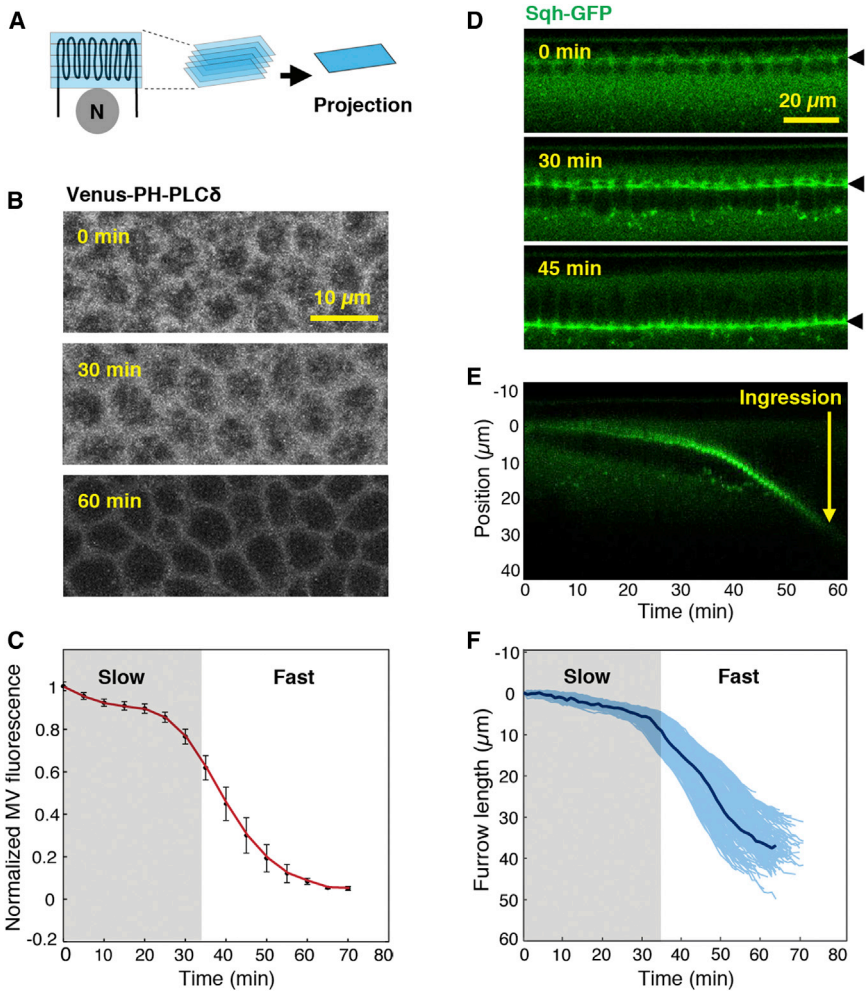

Figure 2. The Kinetics of Microvillar Membrane Depletion and Furrow Ingression Are Biphasic

(A) Schematic showing time-lapse 3D stacks, encompassing the microvilli, are collected and collapsed into projections.

(B) Projections of apical Venus-PH-PLCδ showing depletion of microvillar membrane over time.

(C) Quantification of average normalized apical fluorescence intensity versus time for Venus-PH-PLCδ (n = 8 embryos; mean ± SE). The slow depletion phase is shaded. The solid line is a spline through the data points.

(D) Time-lapse cross-sections of furrow ingression in a Sqh-GFP embryo. Arrowheads indicate the ingression front.

(E) Kymograph of furrow ingression in a Sqh-GFP embryo.

(F) Quantification of furrow ingression from Sqh-GFP embryos (light blue; n = 353 trajectories from 12 embryos). A typical trajectory is highlighted. For (B)–(F), time is from cellularization start.

See also Figures S2 and S3, Table S2, and Movies S1 and S2.

time-lapse (4D) imaging of the apical surface of embryos expressing the membrane marker PLCδ pleckstrin homology domain (Venus-PH-PLCδ; Figures 2A and 2B). Venus-PH-PLCδ binds PtdIns(4,5)P_2 in the plasma membrane, and labels apical microvilli (Figure 2B; Figure S2A; Stauffer et al., 1998). For each time frame, image stacks encompassing the microvilli were collapsed into maximum-intensity projections, and fluorescence intensity was quantified (Figures 2A–2C). Unexpectedly, we found that the depletion of microvillar membrane is biphasic during cellularization. Specifically, membrane is depleted slowly at first and rapidly later on (n = 8 embryos). Palmitoylated membrane probes Gap43-mCherry and Casein Kinase-1/Spider-GFP showed the same kinetics (n = 7 embryos each; Figures S2B–S2D). Thus, we conclude that microvillar membrane is depleted in a slow then fast phase during cellularization.

Currently, there is no consensus regarding the kinetics of furrow ingression during cellularization. Depending on the report, furrows display up to four qualitatively defined ingression phases, with the transition from a slow to a fast ingression velocity occurring at 5–12 μm furrow length and 25–44 min after cellularization starts (Foe et al., 1993; Lecuit and Wieschaus, 2000; Sommi et al., 2010). Because microvillar membrane depletion also followed complex kinetics, with a slow and fast phase, we suspected a relationship with furrow ingression. To define furrow kinetics, we imaged ingression at the cross-section of live embryos expressing Myosin-2 regulatory light chain/Spaghetti Squash-GFP (Sqh-GFP; Royou et al., 2004). Sqh-GFP marks furrow tips, and so forms a moving front during ingression (Figures 2D and 2E; Movie S1). To ensure imaging of the entire cellularization process, we collected data from the preceding furrow regression at mitotic cycle 13 through gastrulation, which immediately follows. Using automated software to measure the position versus time, or x(t), trajectory for many furrows per embryo (Figure 2F; Movie S2), we found that the most robust feature of ingression is a slow-velocity phase followed by a fast-velocity phase, with the transition at 5.7 ± 0.2 μm furrow length and 33.8 ± 0.6 min after cellularization onset (n = 353 trajectories from 12 embryos; mean ± SE; Figures S3A and S3B; Table S2). Thus, like microvillar membrane depletion, furrow ingression is biphasic, starting at a slow velocity and switching to a faster one.

Are the biphasic kinetics of depletion and ingression coupled? If so, the microvillar membrane decrease should be in sync with furrow length increase. To test this, we related the 4D depletion data to furrow length, using the x(t) ingression parameters to make the time-to-length conversion. We found that microvillar membrane is depleted linearly with increasing furrow length throughout cellularization (Figure 3A; Figures S3C and S3D). We next asked whether the linear relationship between microvillar depletion and furrow length could be detected by direct imaging of the microvilli themselves. We used SEM of fractured embryos to examine the density of microvilli over the course of cellularization (Figure 1B). Again, microvillar density decreased linearly with increasing furrow length (Figure 3B), suggesting

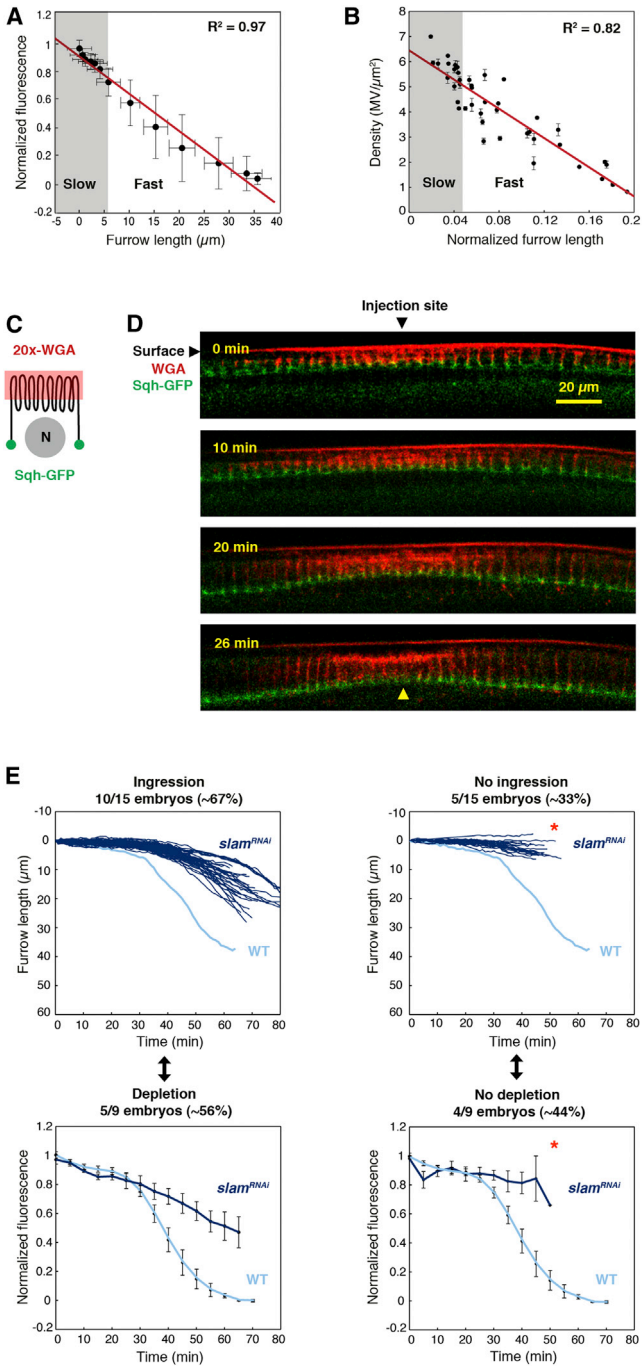

Figure 3. Furrow Ingression Controls the Kinetics of Microvillar Membrane Depletion

(A) Quantification of average normalized fluorescence intensity of microvillar membrane versus furrow length for Venus-PH-PLCδ (n = 8 embryos; mean ± SD).

(B) Quantification of microvillar density versus normalized furrow length (n = 42 embryos; mean ± SE). Furrow length is normalized to embryo diameter to correct for embryo shrinkage upon fixation. For (A) and (B), the line is a linear least-square fit.

(C) Schematic showing 20x-WGA^{AX594} applied to crosslink apical microvillar membrane in Sqh-GFP embryos.

(D) Time-lapse cross-sections showing an immobilized patch of apical membrane (20x-WGA^{AX594}; red) at the perivitelline injection site. Sqh-GFP (green) marks furrow tips. Furrows under the patch (arrowhead) are shorter than in regions distal to the patch (50.9% ± 6.4% shorter in this embryo; n = 3 furrows per region; mean ± SD).

(E) Quantification of furrow ingression for *slam*^{RNAi} in Sqh-GFP embryos (dark blue; ingression, 46 trajectories from eight embryos; no ingression, 25 trajectories from five embryos) with corresponding behaviors in microvillar membrane depletion for *slam*^{RNAi} in Venus-PH-PLCδ embryos (depletion, five embryos; no depletion, four embryos; mean ± SE). Wild-type ingression and depletion are shown in light blue for comparison (see Figure 2). Asterisks indicate when cortical disintegration occurred, preventing further analysis of kinetics.

See also Figure S4.

that membrane is liberated for furrow growth via the disassembly of more and more microvilli.

Microvilli Provide Membrane for Ingression

To further understand the link between microvillar depletion and furrow growth, we manipulated the extent of microvillar disassembly and looked for a reciprocal change in furrow length. Previously, Abelson kinase mutants (*abl*$^{-}$) were shown by SEM to maintain dense microvilli, even at the end of cellularization (Grevengoed et al., 2003). We used maternally induced *abl* RNAi (Ni et al., 2011), and acquired projected cross-sections of fluorescently labeled microvilli from fixed embryos. As expected from genetic mutants, we saw microvilli maintained in late-cellularizing *abl* RNAi embryos (*abl*^{RNAi}; Figure S4A). Final furrow lengths in *abl*^{RNAi} embryos were also significantly shorter than controls (30.5 ± 0.8 μm in *abl*^{RNAi} versus 36.8 ± 0.7 μm in controls; mean ± SE; n = 10 embryos each). These results suggest that membrane is aberrantly retained in the microvilli of *abl*^{RNAi} mutants at the expense of furrow growth.

However, *abl*^{RNAi} mutants have reduced F-actin levels at the furrow (Grevengoed et al., 2003), which may impact final furrow length. To circumvent this concern, we manipulated microvillar membrane depletion by another method. We crosslinked the apical cell surface by injecting a high concentration of red fluorescent wheat germ agglutinin (20x-WGA^{AX594}) into the perivitelline space of Sqh-GFP embryos during the slow phase of cellularization (Figure 3C; Lecuit and Wieschaus, 2000; Sokac and Wieschaus, 2008a). Because WGA is heterodimeric, injection at high concentration (>1 mg ml^{-1}) crosslinks glycosylated transmembrane proteins within a small area, creating a patch of red membrane with limited mobility (Figure 3D; Canman and Bement, 1997). We found that furrows under the patch failed to ingress to the same extent as their neighbors, causing a bowing of the ingression front (n = 4 of 7 embryos). We did not see any inhibition of furrow ingression for injections done at low concentrations of WGA^{AX594} (1x-WGA^{AX594}; see below and Table S2). Thus, consistent with the *abl*^{RNAi} observations, these results support the idea that membrane for furrow ingression comes from the microvilli.

Furrow Ingression Controls the Kinetics of Microvillar Depletion

Given that the kinetics of microvillar depletion are coupled to furrow ingression, and the microvilli appear to be a membrane source for furrows, we wondered whether furrow ingression controls microvillar disassembly. We manipulated furrow

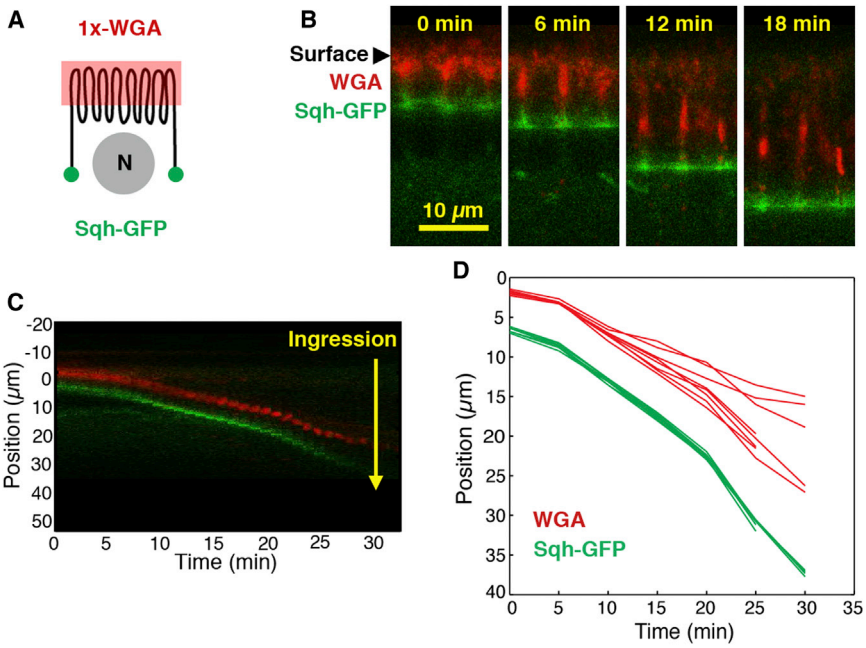

Figure 4. Microvillar Membrane Moves into Ingressing Furrows

(A) Schematic showing 1x-WGA^{AX594} applied to label apical microvillar membrane in Sqh-GFP embryos.

(B) Time-lapse cross-sections showing microvillar membrane (1x-WGA^{AX594}; red) move into ingressing furrows. Sqh-GFP (green) marks furrow tips.

(C) Kymograph showing the trajectory of microvillar membrane (1x-WGA^{AX594}; red) in one furrow of a Sqh-GFP (green) embryo.

(D) Quantification of position versus time trajectories for Sqh-GFP (green) and 1x-WGA^{AX594} (red) (n = 8 furrows from one embryo).

(E) Time-lapse cross-sections showing microvillar membrane (1x-WGA^{AX594}; red) fails to ingress in a "no ingression" *slam*^{RNAi} embryo. Sqh-GFP (green) marks the furrow tips, which barely ingress during imaging. The asterisk indicates when cortical disintegration occurred. For (B)–(E), time is from imaging start.

See also Table S2.

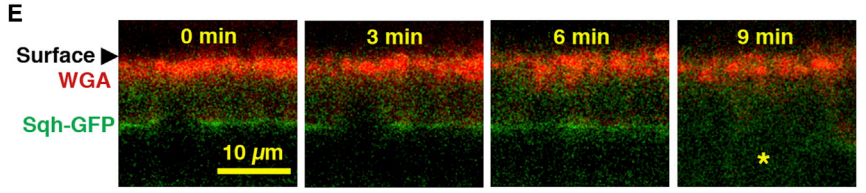

ingression kinetics using *slam* RNAi (*slam*^{RNAi}) and looked for changes in microvillar membrane depletion. Slam localizes to furrow tips, interacts biochemically with RhoGEF2, and is required for recruitment of RhoGEF2, Rho1-GTPase, and Myosin-2 to furrow tips, and *slam*-null or *slam*^{RNAi} embryos show severely perturbed furrow ingression (Lecuit et al., 2002; Stein et al., 2002; Wenzl et al., 2010). We found that the extent of microvillar membrane depletion is reduced in *slam*^{RNAi} compared to buffer-injected controls, and correlates with shorter furrow lengths (apical Venus-PH-PLCδ depletion 29.0% ± 3.6% in *slam*^{RNAi} versus 50.7% ± 2.2% in controls; furrow length 18.6 ± 1.9 μm in *slam*^{RNAi} versus 36.9 ± 0.5 μm in controls; mean ± SE; n ≥ 4 embryos each). We then examined furrow ingression kinetics in Sqh-GFP embryos following *slam*^{RNAi}. Within an embryo, a majority of the tractable furrows (n ≥ 3 trajectories) displayed similar dynamics. We categorized ingression behaviors per embryo as either "ingression" or "no ingression" (Figure 3E). Consistent with this, we observed either depletion or no depletion of microvillar membrane in Venus-PH-PLCδ embryos with *slam*^{RNAi} (Figure 3E), and the distribution of embryos showing each ingression/depletion behavior roughly matched (Figure 3E). So, for *slam*^{RNAi} and *abl*^{RNAi} manipulations, a change in the extent or rate of microvillar membrane depletion was accompanied by a reciprocal and proportionate change in furrow ingression rate and/or length. For *slam*^{RNAi}, these data argue that the rate of furrow ingression governs the rate of microvillar membrane depletion.

Microvillar Membrane Is Pulled Directly into Ingressing Furrows

We next asked how microvillar membrane is transferred to ingressing furrows. We envisioned two possible mechanisms: microvillar membrane could be endocytosed and later exocytosed at the growing furrow, similar to trafficking pathways reported for cell division in cultured cells and plants (Dhonukshe et al., 2006; Schweitzer et al., 2005). Alternatively, microvillar membrane could be unfolded and pulled along the plane of the plasma membrane into growing furrows. We used pulse-chase, time-lapse imaging to follow the redistribution of labeled microvillar membrane. We injected a low concentration of WGA^{AX594} (1x-WGA^{AX594}) into the perivitelline space of Sqh-GFP embryos during the slow-velocity phase of cellularization (Figure 4A). Upon injection, WGA^{AX594} immediately bound to a small area of the apical membrane, effectively creating a pulse of labeling. Once bound, 1x-WGA^{AX594} either remains on the plasma membrane or can be endocytosed (Lecuit and Wieschaus, 2000; Sokac and Wieschaus, 2008a).

In snapshot views, apical 1x-WGA^{AX594}-labeled membrane redistributed to the furrows, as previously described (Figure 4B; Lecuit and Wieschaus, 2000). We then did time-lapse imaging to follow the kinetics and path of redistribution. Sqh-GFP signal allowed simultaneous imaging of furrow ingression. The predominant behavior observed was 1x-WGA^{AX594} membrane moving along the cell surface, entering furrows, and ingressing with the same kinetics as Sqh-GFP (n = 7 embryos; Figures 4B–4D). Although minor variations in 1x-WGA^{AX594} ingression behaviors were observed between different furrows (Figure 4D), the front of the 1x-WGA^{AX594} membrane was strikingly coupled with the ingressing furrow tips (Figure 4D).

We occasionally saw incorporation of apical 1x-WGA^{AX594} into endocytic vesicles (0.4 ± 0.2 vesicles per min over ~75 μm of apical surface; mean ± SD; n = 3 embryos). However, the number

of endocytic events was significantly less than what would be required to consume all the microvilli according to the rates of membrane depletion that we determined above (compare to the calculated value of 8.3 ± 2.7 vesicles per min per μm^2 of apical surface; mean ± SD). To directly test for the role of endocytosis in membrane transfer, we repeated the pulse-labeling assay in the background of a temperature-sensitive allele of *dynamin* (*shibire*^{ts}; Sqh-GFP). We found that ingression velocity is slightly slower in *shibire*^{ts}; Sqh-GFP embryos at restrictive temperature (Table S2; Pelissier et al., 2003; Su et al., 2013); however, apical microvillar membrane is still efficiently transferred to the furrows in these embryos (Figure S4B). This result argues against endocytosis playing a major role in the transfer of microvillar membrane to furrows. Instead, our observations support a path by which microvillar membrane moves along the plasma membrane and into ingressing furrows.

Finally, to test whether furrow ingression itself drives the transfer of microvillar membrane into furrows, we injected 1x-WGA^{AX594} into the perivitelline space of *slam*^{RNAi} embryos at midcellularization and did time-lapse imaging. Because many *slam*^{RNAi} embryos show severely compromised furrow ingression, this allowed us to observe at the single-embryo level how microvillar membrane depletion is linked to furrow ingression. As above, we could categorize the ingression behaviors per embryo as either "ingression" or "no ingression": in embryos where furrow ingression proceeded, 1x-WGA^{AX594} was transferred to the furrows. In embryos with no significant ingression, 1x-WGA^{AX594} remained apical (Figure 4E). In all *slam*^{RNAi} embryos (n = 5), the behavior of the furrows dictated the behavior of microvillar membrane, supporting our model that ingression drives disassembly of the microvilli and pulls microvillar membrane into the furrows.

DISCUSSION

Here we show that microvillar membrane depletion and furrow ingression are linearly coupled throughout all of cellularization. This argues against previous theories that microvilli fuel one phase of cellularization whereas some distinct membrane source fuels another (Fullilove and Jacobson, 1971; Sommi et al., 2010). That is, our data do not easily accommodate any model wherein a mechanistic switch from a solely microvillar to exocytic membrane source governs the biphasic kinetics of cellularization. Instead, we believe that the biphasic kinetics reflect a change at the actomyosin furrow tips. Specifically, we find that the switch from slow phase to fast phase occurs at ~5 μm furrow length coincident with (1) the completion of assembly of the furrow tip domain (i.e., furrow canal; Grosshans et al., 2005; Padash Barmchi et al., 2005; Sokac and Wieschaus, 2008b) and (2) cessation of endocytosis from furrow tips, which promotes faster ingression (Sokac and Wieschaus, 2008a; Su et al., 2013; Yan et al., 2013). Thus, we suggest that the switch from slow to fast phase, for both microvillar depletion and furrow ingression, is governed by events taking place at the furrows.

We estimate that microvilli can store at least half of the membrane required for furrow ingression, which is in agreement with other studies that also demonstrate a role for exocytosis during cellularization (Burgess et al., 1997; Lecuit and Wieschaus, 2000; Murthy et al., 2010; Pelissier et al., 2003; Riggs et al., 2003; Schulze and Bellen, 1996). For example, mutations in exocytic machinery cause furrow ingression defects (Burgess et al., 1997; Murthy et al., 2010), as does blocking Golgi traffic (Sisson et al., 2000). Several studies suggest that the bulk of exocytosis occurs on the apical and/or apicolateral cell surface near adherens junctions: syntaxin and exocyst component Sec5 are enriched apically during cellularization (Burgess et al., 1997; Murthy et al., 2010), and Golgi bodies move toward the apical cell surface (Pelissier et al., 2003; Sisson et al., 2000). Certainly, our time-lapse 1x-WGA^{AX594} data are consistent with an earlier proposal that apical insertion of Golgi-derived membrane contributes to the flow of microvillar membrane toward furrows (Lecuit and Wieschaus, 2000).

How does apical insertion relate to microvillar architecture? Recently, it was reported that the microvilli on cellularizing embryos are not static but instead protrude and retract rapidly (Fabrowski et al., 2013). We suggest that apical exocytosis contributes excess membrane to the apical surface, and that membrane can either be pruned away via endocytosis or, alternatively, stored in dynamic microvillar protrusions prior to translocation into the furrows. We believe that this model both unifies the current cellularization literature and is in agreement with emerging themes for cell-shape change including the significant roles played by (1) plasma membrane folding and unfolding and (2) the antagonism between actin polymerization and membrane tension.

For example, our data suggest that furrow ingression pulls or puts tension on the apical plasma membrane, driving the unfolding of microvilli. Contrary to the idea that plasma membrane remodeling is exclusively mediated by exo- or endocytosis (Deschamps et al., 2013), microvillar unfolding suggests that the plasma membrane alone has the material reserves and plasticity to make a critical contribution to cell-shape change. This is in line with theoretical models (Herant et al., 2005; Sommi et al., 2010) and recent findings for other cell-surface specializations: first, caveolar pits at the plasma membrane of mammalian cultured cells disassemble, independent of endocytosis, to liberate membrane upon cell stretching (Sinha et al., 2011). Second, in spreading fibroblasts, surface folds and blebs also flatten out within the plane of the plasma membrane as membrane lamellipodia form. Only once the folds are exhausted does membrane addition by exocytosis start (Gauthier et al., 2011). A similar mechanism is employed during phagocytosis in transformed macrophages (Masters et al., 2013). Third, plasma membrane blebs and rounded protrusions that drive amoeboid-like motility and promote reliable cytokinesis expand and contract at timescales incompatible with remodeling by exo- and endocytosis (Charras et al., 2005; Kapustina et al., 2013; Sedzinski et al., 2011). Now our study extends this theme from cells in a dish to a morphogenetic event in an intact embryo. Given the reports of microvilli and blebs forming and retracting during blastomere compaction in mice, ventral furrow formation in flies, and so forth (Ducibella et al., 1977; Martin et al., 2010), we expect that the plasma membrane can serve as an autonomous facilitator of cell-shape change during morphogenesis in many organisms and in many contexts.

Finally, our findings suggest that microvilli are disassembled on demand when the need for membrane in the furrows arises. What is the signal for disassembly? Is it molecular or

mechanical? We imagine that the most likely signal for disassembly comes from the antagonistic relationship between membrane tension and the actin cytoskeleton. Although microvilli could be disassembled by apical endocytosis during cellularization (our data and Fabrowski et al., 2013), the resulting endosomes make no clear contribution to furrow ingression (Fabrowski et al., 2013), consistent with our results that endocytosis is not required for the transfer of membrane from microvilli to furrows. Instead, drawing on lessons from filopodia, phagocytic cups, and the leading edge of motile cells (Gauthier et al., 2009; Ji et al., 2008; Keren et al., 2008; Masters et al., 2013; Mogilner and Rubinstein, 2005; Raucher and Sheetz, 2000), we suggest that high plasma membrane tension, generated by the pulling forces of furrow ingression, could be sufficient to limit and/or stall actin polymerization at microvillar tips (Tyska and Mooseker, 2002). In this way, furrow ingression itself would act as the signal to both promote microvillar disassembly and prevent assembly of new microvilli. Thus, this work resets the bar on an old idea; we now need to understand how the actin and membrane systems talk to each other to signal and orchestrate the microvillar unfolding that fuels cell-surface growth.

EXPERIMENTAL PROCEDURES

SEM

Embryos were fixed (Martin et al., 2010) and fractured with a needle. Dry samples were mounted on double-stick carbon tabs (Ted Pella), coated under vacuum with platinum alloy, and then immediately flash carbon coated. Samples were imaged using a JSM-5910 scanning electron microscope (JEOL) at an accelerating voltage of 5 kV.

Embryo Injections

Approximately 50 pl of *slam* dsRNA was injected into freshly laid embryos (Lecuit et al., 2002). *slam* RNAi controls were buffer injected. For WGA injections, 50 pl of Alexa594-WGA (0.1 or 2 mg ml^{-1} in PBS; Life Technologies) was injected into the perivitelline space at the indicated cellularization phase (Sokac and Wieschaus, 2008a).

Live Imaging

Embryos were mounted (Figard and Sokac, 2011) and imaged at 19°C on a Zeiss LSM 710 microscope with a 40× water-immersion objective (NA 1.2) and pinhole of 1 arbitrary unit. For furrow ingression and WGA tracking, images were acquired at the midplane at 1 or 2 min intervals. For 4D imaging, z stacks spanning ~5 μm of apical surface were collected every 5 min.

SUPPLEMENTAL INFORMATION

Supplemental Information includes Supplemental Experimental Procedures, four figures, two tables, and two movies and can be found with this article online at http://dx.doi.org/10.1016/j.devcel.2013.11.006.

ACKNOWLEDGMENTS

We thank Leonardo Sepúlveda, Sam Skinner, and Mengyu Wang (Baylor College of Medicine) for assistance with data analysis; Eric Wieschaus (Princeton University), Adam Martin (MIT), and Vanaja Konduri (Baylor College of Medicine) for flies; Kenneth Dunner, Jr. (MD Anderson Cancer Center) for SEM support; and Bill Bement (University of Wisconsin-Madison) and Herbert Levine (Rice University) for discussing results. A.M.S. and L.F. are supported by a Computational and Integrative Biomedical Research Center Seed Award and Curtis Hankamer Basic Research Fund Award (Baylor College of Medicine). Support for I.G. and H.X. was provided by NIH grant R01GM082837, NSF grants 082265 (Physics Frontiers Center: Center for the Physics of Living Cells) and PHY-1147498 (CAREER), and Welch Foundation grant Q-1759. The High Resolution EM Facility at MD Anderson Cancer Center is supported by NIH Institutional Core Grant CA16672. The TRiP RNAi resource at Harvard Medical School is supported by NIH grant R01GM084947.

Received: April 1, 2013
Revised: August 29, 2013
Accepted: November 6, 2013
Published: December 5, 2013

REFERENCES

Arnold, J.M. (1969). Cleavage furrow formation in a telolecithal egg (*Loligo pealii*). I. Filaments in early furrow formation. J. Cell Biol. *41*, 894–904.

Ashworth, S.L., and Molitoris, B.A. (1999). Pathophysiology and functional significance of apical membrane disruption during ischemia. Curr. Opin. Nephrol. Hypertens. *8*, 449–458.

Bement, W.M., Forscher, P., and Mooseker, M.S. (1993). A novel cytoskeletal structure involved in purse string wound closure and cell polarity maintenance. J. Cell Biol. *121*, 565–578.

Betchaku, T., and Trinkaus, J.P. (1978). Contact relations, surface activity, and cortical microfilaments of marginal cells of the enveloping layer and of the yolk syncytial and yolk cytoplasmic layers of fundulus before and during epiboly. J. Exp. Zool. *206*, 381–426.

Burgess, R.W., Deitcher, D.L., and Schwarz, T.L. (1997). The synaptic protein syntaxin1 is required for cellularization of *Drosophila* embryos. J. Cell Biol. *138*, 861–875.

Canman, J.C., and Bement, W.M. (1997). Microtubules suppress actomyosin-based cortical flow in *Xenopus* oocytes. J. Cell Sci. *110*, 1907–1917.

Charras, G.T., Yarrow, J.C., Horton, M.A., Mahadevan, L., and Mitchison, T.J. (2005). Non-equilibration of hydrostatic pressure in blebbing cells. Nature *435*, 365–369.

DeRosier, D.J., and Tilney, L.G. (2000). F-actin bundles are derivatives of microvilli: What does this tell us about how bundles might form? J. Cell Biol. *148*, 1–6.

Deschamps, C., Echard, A., and Niedergang, F. (2013). Phagocytosis and cytokinesis: do cells use common tools to cut and to eat? Highlights on common themes and differences. Traffic *14*, 355–364.

Dhonukshe, P., Baluska, F., Schlicht, M., Hlavacka, A., Samaj, J., Friml, J., and Gadella, T.W., Jr. (2006). Endocytosis of cell surface material mediates cell plate formation during plant cytokinesis. Dev. Cell *10*, 137–150.

Ducibella, T., Ukena, T., Karnovsky, M., and Anderson, E. (1977). Changes in cell surface and cortical cytoplasmic organization during early embryogenesis in the preimplantation mouse embryo. J. Cell Biol. *74*, 153–167.

Fabrowski, P., Necakov, A.S., Mumbauer, S., Loeser, E., Reversi, A., Streichan, S., Briggs, J.A., and De Renzis, S. (2013). Tubular endocytosis drives remodelling of the apical surface during epithelial morphogenesis in *Drosophila*. Nat. Commun. *4*, 2244.

Figard, L., and Sokac, A.M. (2011). Imaging cell shape change in living *Drosophila* embryos. J. Vis. Exp. *49*, e2503.

Foe, V.E., Odell, G.M., and Edgar, B.E. (1993). Mitosis and morphogenesis in the *Drosophila* embryo: point and counterpoint. In The Development of *Drosophila melanogaster*, M. Bate and V. Hartenstein, eds. (Plainview, NY: Cold Spring Harbor Laboratory Press), pp. 149–300.

Fullilove, S.L., and Jacobson, A.G. (1971). Nuclear elongation and cytokinesis in *Drosophila montana*. Dev. Biol. *26*, 560–577.

Gauthier, N.C., Rossier, O.M., Mathur, A., Hone, J.C., and Sheetz, M.P. (2009). Plasma membrane area increases with spread area by exocytosis of a GPI-anchored protein compartment. Mol. Biol. Cell *20*, 3261–3272.

Gauthier, N.C., Fardin, M.A., Roca-Cusachs, P., and Sheetz, M.P. (2011). Temporary increase in plasma membrane tension coordinates the activation of exocytosis and contraction during cell spreading. Proc. Natl. Acad. Sci. USA *108*, 14467–14472.

Grevengoed, E.E., Fox, D.T., Gates, J., and Peifer, M. (2003). Balancing different types of actin polymerization at distinct sites: roles for Abelson kinase and Enabled. J. Cell Biol. *163*, 1267–1279.

Grosshans, J., Wenzl, C., Herz, H.M., Bartoszewski, S., Schnorrer, F., Vogt, N., Schwarz, H., and Müller, H.A. (2005). RhoGEF2 and the formin Dia control the formation of the furrow canal by directed actin assembly during *Drosophila* cellularisation. Development *132*, 1009–1020.

Herant, M., Heinrich, V., and Dembo, M. (2005). Mechanics of neutrophil phagocytosis: behavior of the cortical tension. J. Cell Sci. *118*, 1789–1797.

Hudspeth, A.J., and Corey, D.P. (1977). Sensitivity, polarity, and conductance change in the response of vertebrate hair cells to controlled mechanical stimuli. Proc. Natl. Acad. Sci. USA *74*, 2407–2411.

Ji, L., Lim, J., and Danuser, G. (2008). Fluctuations of intracellular forces during cell protrusion. Nat. Cell Biol. *10*, 1393–1400.

Kapustina, M., Elston, T.C., and Jacobson, K. (2013). Compression and dilation of the membrane-cortex layer generates rapid changes in cell shape. J. Cell Biol. *200*, 95–108.

Keren, K., Pincus, Z., Allen, G.M., Barnhart, E.L., Marriott, G., Mogilner, A., and Theriot, J.A. (2008). Mechanism of shape determination in motile cells. Nature *453*, 475–480.

Lecuit, T., and Wieschaus, E. (2000). Polarized insertion of new membrane from a cytoplasmic reservoir during cleavage of the *Drosophila* embryo. J. Cell Biol. *150*, 849–860.

Lecuit, T., Samanta, R., and Wieschaus, E. (2002). *slam* encodes a developmental regulator of polarized membrane growth during cleavage of the *Drosophila* embryo. Dev. Cell *2*, 425–436.

Louvard, D., Kedinger, M., and Hauri, H.P. (1992). The differentiating intestinal epithelial cell: establishment and maintenance of functions through interactions between cellular structures. Annu. Rev. Cell Biol. *8*, 157–195.

Martin, A.C., Gelbart, M., Fernandez-Gonzalez, R., Kaschube, M., and Wieschaus, E.F. (2010). Integration of contractile forces during tissue invagination. J. Cell Biol. *188*, 735–749.

Masters, T.A., Pontes, B., Viasnoff, V., Li, Y., and Gauthier, N.C. (2013). Plasma membrane tension orchestrates membrane trafficking, cytoskeletal remodeling, and biochemical signaling during phagocytosis. Proc. Natl. Acad. Sci. USA *110*, 11875–11880.

Mogilner, A., and Rubinstein, B. (2005). The physics of filopodial protrusion. Biophys. J. *89*, 782–795.

Murthy, M., Teodoro, R.O., Miller, T.P., and Schwarz, T.L. (2010). Sec5, a member of the exocyst complex, mediates *Drosophila* embryo cellularization. Development *137*, 2773–2783.

Ni, J.Q., Zhou, R., Czech, B., Liu, L.P., Holderbaum, L., Yang-Zhou, D., Shim, H.S., Tao, R., Handler, D., Karpowicz, P., et al. (2011). A genome-scale shRNA resource for transgenic RNAi in *Drosophila*. Nat. Methods *8*, 405–407.

Padash Barmchi, M., Rogers, S., and Häcker, U. (2005). DRhoGEF2 regulates actin organization and contractility in the *Drosophila* blastoderm embryo. J. Cell Biol. *168*, 575–585.

Pelissier, A., Chauvin, J.P., and Lecuit, T. (2003). Trafficking through Rab11 endosomes is required for cellularization during *Drosophila* embryogenesis. Curr. Biol. *13*, 1848–1857.

Porter, K., Prescott, D., and Frye, J. (1973). Changes in surface morphology of Chinese hamster ovary cells during the cell cycle. J. Cell Biol. *57*, 815–836.

Raucher, D., and Sheetz, M.P. (2000). Cell spreading and lamellipodial extension rate is regulated by membrane tension. J. Cell Biol. *148*, 127–136.

Revenu, C., Athman, R., Robine, S., and Louvard, D. (2004). The co-workers of actin filaments: from cell structures to signals. Nat. Rev. Mol. Cell Biol. *5*, 635–646.

Riggs, B., Rothwell, W., Mische, S., Hickson, G.R., Matheson, J., Hays, T.S., Gould, G.W., and Sullivan, W. (2003). Actin cytoskeleton remodeling during early *Drosophila* furrow formation requires recycling endosomal components Nuclear-fallout and Rab11. J. Cell Biol. *163*, 143–154.

Royou, A., Field, C., Sisson, J.C., Sullivan, W., and Karess, R. (2004). Reassessing the role and dynamics of nonmuscle myosin II during furrow formation in early *Drosophila* embryos. Mol. Biol. Cell *15*, 838–850.

Schroeder, T.E. (1978). Microvilli on sea urchin eggs: a second burst of elongation. Dev. Biol. *64*, 342–346.

Schulze, K.L., and Bellen, H.J. (1996). *Drosophila syntaxin* is required for cell viability and may function in membrane formation and stabilization. Genetics *144*, 1713–1724.

Schweitzer, J.K., Burke, E.E., Goodson, H.V., and D'Souza-Schorey, C. (2005). Endocytosis resumes during late mitosis and is required for cytokinesis. J. Biol. Chem. *280*, 41628–41635.

Sedzinski, J., Biro, M., Oswald, A., Tinevez, J.Y., Salbreux, G., and Paluch, E. (2011). Polar actomyosin contractility destabilizes the position of the cytokinetic furrow. Nature *476*, 462–466.

Shuster, C.B., and Burgess, D.R. (2002). Targeted new membrane addition in the cleavage furrow is a late, separate event in cytokinesis. Proc. Natl. Acad. Sci. USA *99*, 3633–3638.

Sinha, B., Köster, D., Ruez, R., Gonnord, P., Bastiani, M., Abankwa, D., Stan, R.V., Butler-Browne, G., Vedie, B., Johannes, L., et al. (2011). Cells respond to mechanical stress by rapid disassembly of caveolae. Cell *144*, 402–413.

Sisson, J.C., Field, C., Ventura, R., Royou, A., and Sullivan, W. (2000). Lava lamp, a novel peripheral golgi protein, is required for *Drosophila melanogaster* cellularization. J. Cell Biol. *151*, 905–918.

Sokac, A.M., and Wieschaus, E. (2008a). Local actin-dependent endocytosis is zygotically controlled to initiate *Drosophila* cellularization. Dev. Cell *14*, 775–786.

Sokac, A.M., and Wieschaus, E. (2008b). Zygotically controlled F-actin establishes cortical compartments to stabilize furrows during *Drosophila* cellularization. J. Cell Sci. *121*, 1815–1824.

Sommi, P., Ananthakrishnan, R., Cheerambathur, D.K., Kwon, M., Morales-Mulia, S., Brust-Mascher, I., and Mogilner, A. (2010). A mitotic kinesin-6, Pav-KLP, mediates interdependent cortical reorganization and spindle dynamics in *Drosophila* embryos. J. Cell Sci. *123*, 1862–1872.

Stauffer, T.P., Ahn, S., and Meyer, T. (1998). Receptor-induced transient reduction in plasma membrane PtdIns(4,5)P_2 concentration monitored in living cells. Curr. Biol. *8*, 343–346.

Stein, J.A., Broihier, H.T., Moore, L.A., and Lehmann, R. (2002). Slow as molasses is required for polarized membrane growth and germ cell migration in *Drosophila*. Development *129*, 3925–3934.

Su, J., Chow, B., Boulianne, G.L., and Wilde, A. (2013). The BAR domain of amphiphysin is required for cleavage furrow tip-tubule formation during cellularization in *Drosophila* embryos. Mol. Biol. Cell *24*, 1444–1453.

Sundd, P., Pospieszalska, M.K., Cheung, L.S., Konstantopoulos, K., and Ley, K. (2011). Biomechanics of leukocyte rolling. Biorheology *48*, 1–35.

Turner, F.R., and Mahowald, A.P. (1976). Scanning electron microscopy of *Drosophila* embryogenesis. 1. The structure of the egg envelopes and the formation of the cellular blastoderm. Dev. Biol. *50*, 95–108.

Tyska, M.J., and Mooseker, M.S. (2002). MYO1A (brush border myosin I) dynamics in the brush border of LLC-PK1-CL4 cells. Biophys. J. *82*, 1869–1883.

Wenzl, C., Yan, S., Laupsien, P., and Grosshans, J. (2010). Localization of RhoGEF2 during *Drosophila* cellularization is developmentally controlled by Slam. Mech. Dev. *127*, 371–384.

Yan, S., Lv, Z., Winterhoff, M., Wenzl, C., Zobel, T., Faix, J., Bogdan, S., and Grosshans, J. (2013). The F-BAR protein Cip4/Toca-1 antagonizes the formin Diaphanous in membrane stabilization and compartmentalization. J. Cell Sci. *126*, 1796–1805.